# The CANARI HadGEM3 Large Ensemble: Design and evaluation of historical simulations


Reinhard K. H. Schiemann[1], Grenville Lister[1], Rosalyn Hatcher[1], Dan Hodson[1], Bryan Lawrence[1], Len Shaffrey[1], Andrea Dittus[1], Jon Robson[1], Ben Harvey[1], Kevin Hodges[1], Oscar Martínez-Alvarado[1], Steve Woolnough[1], Andrew Turner[1], Simon Wilson[1], Jeff Cole[1], Sharar Ahmadi[1], Laura Baker[1], David Case[1], Steve George[1], Eliza Karlowska[1], Charlotte Lang[1], Annette Osprey[1], Robin Smith[1], Jake Aylmer[2], David Schröder[2], Niamh O'Callaghan[2], Weronika Osmolska[3], Scott Osprey[4], Yevgeny Aksenov[5], Adam T. Blaker[5], Andrew Coward[5], James Harle[5], Jenny Mecking[5], Stephanie Rynders[5], Bablu Sinha[5], Chris Wilson[6], Martin Andrews[7], Steven Hardiman[7], John Rostron[7], David Sexton[7], Hua Lu[8], Tony Phillips[8], Jonny Williams[2,9]

[1]NCAS, University of Reading, UK. [2]Meteorology, University of Reading, UK. [3]NCAS, University of Leeds, UK. [4]NCAS, University of Oxford, UK. [5]NOC, Southampton, UK. [6]NOC, Liverpool, UK. [7]Met Office, Exeter, UK. [8]BAS, Cambridge, UK. [9]NIWA, NZ.


Sharing is encouraged

## 1. Large Ensemble design

As part of the UK national science programme CANARI (Climate Change in the Arctic North Atlantic Region and Impacts on the UK), we have produced a Large Ensemble to address CANARI science questions and as a resource for the community at large. Main characteristics of the new Large Ensemble are:

- Model
  - HadGEM3-GC3.1, the UK Met Office CMIP6 model
  - N216-ORCA0.25 "MM" resolution (~60 km at 50°N, ¼° ocean)
- Experiments
  - CMIP6 historical (1950 – 2014)
  - CMIP6 all-forcing scenario SSP3-7.0 (2015 – 2100)
- 40 ensemble members
  - 5 'macro' x 8 'micro' initialisations
- Output
  - CMIP-like, with boundary conditions for CORDEX-like regions covering most land areas

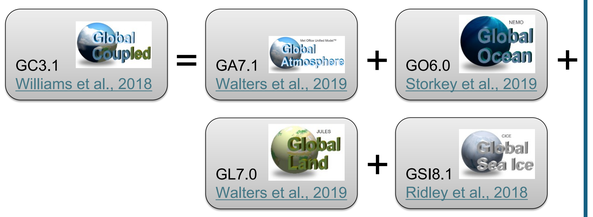


**Figure 1**: HadGEM3-GC3.1 component models and main references.

## 2. Global mean surface temperature

- trend generally consistent with observations (Fig. 2)
- somewhat faster cooling (1950-1970) and warming (1970-2014) in the CANARI Large Ensemble than in observations

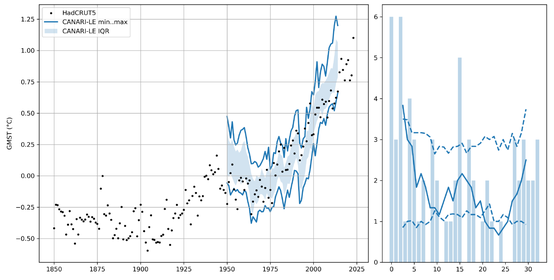


**Figure 2**: (left) Global mean surface temperature anomaly (from 1961-1990) in HadCRUT5 (black dots) and the CANARI Large Ensemble (blue). (right) Ranked histogram. Methods as in Suarez-Gutierrez et al. 2021.

## 3. North Atlantic tropospheric circulation

- good representation of mean eddy-driven jet, including the tilt (Fig. 3a)
- ERA5 strengthening of the jet (Fig. 3c) not seen in the LE (Fig. 3b,d,e)
- ERA5 trend *since 1979* is small and consistent with the LE (Fig. 3d,e)
- interannual variability of jet speed close to ERA5 (Fig. 3f)
- mean intensity of extratropical cyclones well represented, with small negative bias over subpolar gyre region (Fig. 4a)
- cyclone intensity trend consistent between ERA5 and LE (Fig. 4b,c), yet both signs are seen in the LE (Fig. 4e)

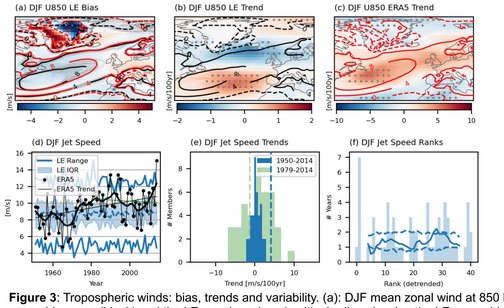


**Figure 3**: Tropospheric winds: bias, trends and variability. (a): DJF mean zonal wind at 850 hPa (U850) in ERA5 (red), the LE ensemble mean (black) and the LE members (grey), with shading showing the LE ensemble mean bias. (b): Ensemble mean U850 trend in the LE over 1950-2014. (c): U850 trend in ERA5 over 1950-2014 (note wider colourbar than b). (d): Time series of 0-60W jet speed in ERA5 (black) and the LE (blue; with median, interquartile range and full range indicated), the 11-year lowess smoothed ERA5 timeseries (thick black) and the 1950-2014 and 1979-2014 linear trends in ERA5 (black, green). (e): Histogram of jet speed linear trends over 1950-2014 (blue) and 1979-2014 (green) and the corresponding ERA5 trends (dashed). (f): Rank histogram for the detrended jet speed timeseries.

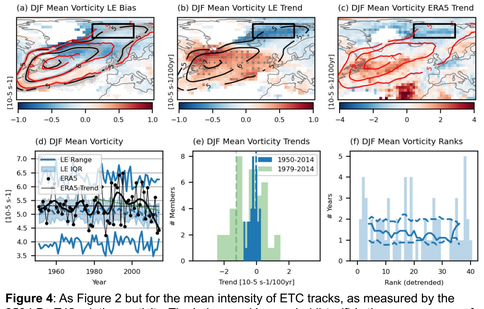


**Figure 4**: As Figure 2 but for the mean intensity of ETC tracks, as measured by the 850 hPa T42 relative vorticity. The index used in panels (d) to (f) is the area average of the mean intensity field over the box indicated in the maps.

## 4. Stratospheric circulation

- winter troposphere/stratosphere zonal mean close to ERA5 with small variation between LE members (Fig. 5)
- stratospheric polar vortex (SPV) too weak/narrow in the upper stratosphere and too strong/broad in the lower stratosphere; Subtropical Westerly Jet also too strong (Fig. 5)
- Number of ERA5 Sudden Stratospheric Warmings (SSWs) within $2\sigma$ of that of the LE (Fig. 6a), with biases in the frequencies closely related to biases in the evolution of the SPV at 60°N, 10hPa (not shown).
- SSW-Northern Annular Mode relationship similar in LE and ERA5; tropospheric descent appears weaker in LE (Fig. 6b,c).

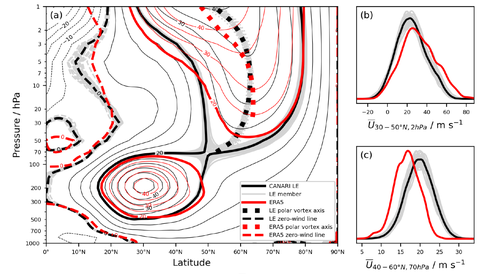


**Figure 5**: **a)** DJF zonal-mean zonal wind $\overline{U}$ (m s−1) (red: ERA5; black CANARI LE; grey: individual LE members. The dotted lines indicate the axis of the stratospheric polar vortex. i.e. where $\overline{U}$ peaks, while the dashed lines are the zero-wind line. The 20 m s$^{-1}$ contours are thickened to highlight the stratospheric polar vortex and the tropospheric subtropical jet. **b)** probability distribution of $\overline{U}_{30-50\text{-}N,2hPa}$ estimated based on ERA5 (red) and CANARI LE (black and gray). (c) same as (b) except for $\overline{U}_{40-60\text{-}N,70hPa}$.

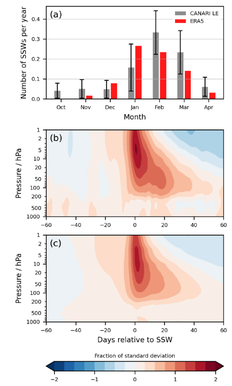


**Figure 6**: **a)** number of SSWs per year from ERA5 (red) and CANARI LE (grey) with whiskers indicating the 2-standard deviation range. The SSWs are identified based on the methodology of Charlton and Polvani (2007). In total, 49 SSWs in ERA5 (1959-2023) while 2329 SSWs in LE. **b)** and **c)** Composite evolution of SSW signal in the NAM for the 60 days before and after the SSW starting date (lag = 0) and over the height range of 1 - 1000 hPa in ERA5 (b) and CANARI LE (c). The NAM is estimated based on the standardised zonal-mean geopotential height anomalies over the polar cap, i.e. 60-90°N.

## 5. Atlantic Meridional Overturning Circulation

- During 2004-2015, the CANARI LE AMOC is somewhat weaker (~1.7 Sv) and less variable (~0.1 Sv) than observations (Fig 7a).
- CANARI LE AMOC peaks around 1980, then declines, consistent with a response to anthropogenic forcing, particularly aerosols (Robson et al. 2022)
- The 1980-2014 decline in the AMOC ranges between -0.5 to -1.6 Sv/decade across the ensemble members; highlighting the large role of internal variability in shaping decadal-to-multidecadal change in this model.
- Northward heat transport similar to AMOC, a little weaker than in RAPID (Fig. 7c)

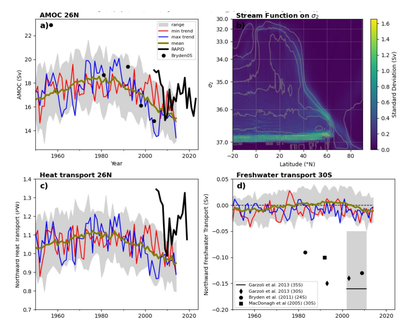


**Figure 7**: **a)** AMOC at 26°N (Sv). Olive green: ensemble mean. Shading is the ensemble range. Red (blue) member with least (greatest) AMOC decline over 1980-2014: -0.5 (-1.6) Sv/decade. Black line: Observed AMOC (RAPID). Black dots: Observed AMOC (Bryden et al., 2005). **b)** AMOC stream function on density levels ($\sigma_2$) (Sv) in grey contours, ensemble standard deviation of time mean (1950-2014) in colours. **c)** Atlantic Ocean Heat transport at 26°N (PW). Red (blue) member with weakest (strongest) AMOC decline as in a) also shading as a). Black: observed heat transport from RAPID (Moat, 2024). **d)** As c, but for Northward Freshwater Transport ($F_{ov}$) at 30°S (colours and shading as c). The uncertainty range for the Garzoli et al. (2013) estimate extends below the y-axis minimum. Black symbols: $F_{ov}$ estimates from observational studies (Garzoli et al. (2013), McDonagh and King (2005), Bryden et al. (2011)). 35°S estimate shows the 2002-2011 time mean and range.

## 6. Arctic Sea Ice

- CANARI LE sea ice extent in 1979-2014 consistent with observations in terms of mean values, seasonal cycle, and trend (Fig. 8a,b)
- Sea-ice volume in CANARI LE rather high compared to an observation-based estimate (PIOMAS; Fig. 8c)
- close relationship between Arctic sea ice decline and warming, and large internal variability over a 35-year period in both (Fig. 8d)
- Members with the most accurate sea-ice decline overestimate the observed temperature increase, which is consistent with the positive sea-ice volume bias in the CANARI LE (Fig. 8d) as greater warming is required to melt more ice.

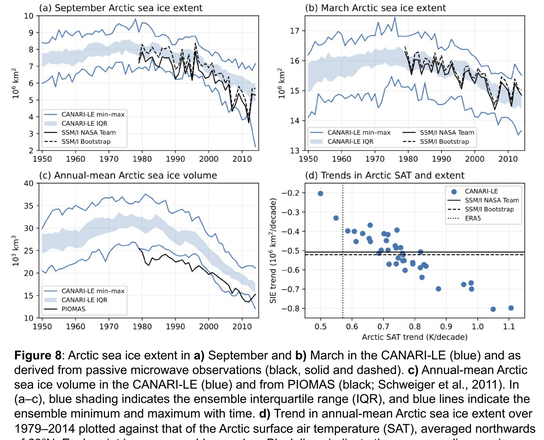


**Figure 8**: Arctic sea ice extent in **a)** September and **b)** March in the CANARI-LE (blue) and as derived from passive microwave observations (black, solid and dashed). **c)** Annual-mean Arctic sea ice volume in the CANARI-LE (blue) and from PIOMAS (black; Schweiger et al., 2011). In (a–c), blue shading indicates the ensemble interquartile range (IQR), and blue lines indicate the ensemble minimum and maximum with time. **d)** Trend in annual-mean Arctic sea ice extent over 1979–2014 plotted against that of the Arctic surface air temperature (SAT), averaged northwards of 60°N. Each point is one ensemble member. Black lines indicate the corresponding sea ice trends from passive microwave observations (solid, dashed) and from ERA5 (dotted).